ELECTRONIC PROPERTIES
OF SOLID

Electronic Structure, Magnetic Properties, and Mechanism of the Insulator−Metal Transition in LaCoO₃ Taking into Account Strong Electron Correlations

S. G. Ovchinnikov[a,b,c], Yu. S. Orlov[a,*], I. A. Nekrasov[d], and Z. V. Pchelkina[e]

[a]Kirenskii Institute of Physics, Siberian Branch, Russian Academy of Sciences, Krasnoyarsk, 660036 Russia
[b]Siberian Federal University, Krasnoyarsk, 660041 Russia
[c]Siberian Aerospace University, Krasnoyarsk, 660014 Russia
[d]Institute of Electrophysics, Ural Division, Russian Academy of Sciences, Yekaterinburg, 620016 Russia
[e]Institute of Metal Physics, Ural Division, Russian Academy of Sciences, Yekaterinburg, 620990 Russia
*e-mail: jso.krasn@mail.ru
Received May 17, 2010

Abstract—The electronic structure of LaCoO₃ at finite temperatures is calculated using the LDA+GTB method taking into account strong electron correlations and possible spin crossover upon an increase in temperature. Gap states revealed in the energy spectrum of LaCoO₃ reduce the dielectric gap width upon heating; this allowed us to describe the insulator−metal transition observed in this compound at $T = 500−600$ K. The temperature dependence of the magnetic susceptibility with a peak at $T \approx 100$ K is explained by the Curie contribution from thermally excited energy levels of the Co^{3+} ion. At high temperatures, the Pauli contribution from a band electron is added and the total magnetization of LaCoO₃ is considered as the sum $M_{tot} = M_{loc} + M_{band}$. The second term describes the band contribution appearing as a result of the insulator−metal transition and facilitating the emergence of a high-temperature anomaly in the magnetic susceptibility of LaCoO₃.

1. INTRODUCTION

Cobaltites of rare-earth metals with the general chemical formula LnCoO₃, where Ln stands for lanthanum (La) or a lanthanide (Gd, Ho, Eu, Sm, etc.), as well as compounds with an alkali-earth element partly substituted for a lanthanide, have been objects of intense studies for more than three decades as materials with clearly manifested physical properties [1] such as colossal magnetoresistance [2], high-temperature ferromagnetism [3], charge ordering [4], electronic phase separation [5], metal−insulator transitions [6], memory effects [7], a cascade of magnetic transitions [8], and the formation of giant polarons [9]. In addition, prospects for practical application of these materials as cathodes in solid-state power supplies have been outlined recently. The basic representative of this cobaltite series is LaCoO₃ with the valence formula $La^{3+}Co^{3+}O_3^{2−}$.

The LaCoO₃ compound has attracted the attention of researches for the first time owing to a peculiar temperature dependence of its magnetic susceptibility $\chi(T)$ [10], which has two broad peaks at $T_1 \approx 100$ K and $T_2 = 500−600$ K. The high-temperature anomaly in the magnetic susceptibility of LaCoO₃ is accompanied by a smooth insulator−metal transition in its conduction, indicating delocalization of charge carriers [11,

12]. A substantial decrease in resistance is also observed in the temperature range above 500 K. It should be noted that the emergence of a high-temperature singularity is often attributed in the literature to the transition to the conducting state. Analysis of scattering of polarized neutrons [13] in LaCoO₃ shows that cobalt ions at low temperatures are in a nonmagnetic low-spin state, while heating changes this to the paramagnetic state. The competition between the low-spin ($^1A_1$), t_{2g}^6, high-spin ($^5T_2$), $t_{2g}^4 e_g^2$, and intermediate-spin ($^3T_1$), $t_{2g}^5 e_g^1$ states of Co^{3+} ion is responsible for the main features of the magnetic, structural, and transport properties of rare-earth cobaltites. In earlier publications, it was initially assumed that the low-spin state is formed instead of the high-spin state due to the presence of the crystal field for the d^6-configuration of the Co^{3+} ion, the energy interval between these states being determined by the spin gap $\Delta_S = E(HS) − E(LS)$ ~ 100 K. Thermal population of the high-spin state ensures a rapid increase in the magnetic susceptibility with a peak near 100 K. The substantial difference between the spin gap and the electrical conduction activation energy $E_a \approx 0.1$ eV for low temperatures implies that LaCoO₃ is not a simple band insulator [11]. Moreover, a considerable difference between charge gap $2E_a \approx 2300$ K and the temperature $T_{IMT} \approx$

600 K of the insulator−metal transition indicates that the latter can hardly be explained in the model of a narrow-gap semiconductor [14].

In spite of the large number of publications devoted to problems of magnetic susceptibility and the insulator−metal transition in $LaCoO_3$, it should be admitted that no consensus has been reached in theoretical or experimental results. This necessitates further investigations. We propose a theoretical description of this transition taking into account strong electron correlations (SECs) playing an important role in the formation of various properties of transition metal oxides. Traditional one-electron approaches do not provide a description for many of these properties; in addition, the fact that the orbital, spin, charge, and lattice degrees of freedom must be taken into account in describing these properties becomes more and more obvious. Usually, the electron−electron interaction is described even in multielectron model using at best the Kanamori approximation, in which the density−density and exchange interactions are preserved from the entire set of the Coulomb matrix elements. The importance of taking into account the total Hamiltonian for the electron−electron interaction is emphasized and substantiated in [15], where its role in the formation of the Mott−Hubbard energy gap,

$$U(d^n) = E(d^{n-1}) + E(d^{n+1}) - 2E(d^n),$$

was demonstrated. The Hubbard parameter U is determined the better, the more accurately and correctly we determine the set of energy levels for the d^{n-1}-, d^n-, and d^{n+1}-configurations of the transition metal ion. This becomes especially important in the presence of crossovers between multielectron energy levels upon a variation of certain external conditions (e.g., pressure or temperature). It was shown in [16] how the spin crossovers change the value of $U(d^n)$ and affect the Mott−Hubbard transition. One of appropriate ways of considering such systems, which takes into account the necessary remarks, is the generalized tight binding (GTB) method [17] and its ab initio version LDA + GTB [18], which are in fact the implementation of the Hubbard ideas for multielectron and multiorbital systems. In Section 2, we briefly describe the main concepts of this method. The Vanier functions are constructed and the parameters of the multiorbital p−d-model are calculated in Section 3 using ab initio LDA calculations. The results of the LDA + GTB calculations of the electronic structure of $LaCoO_3$ are presented in Section 4. Section 5 is devoted to electronic properties. The behavior of the magnetic susceptibility and its features are considered in Section 6.

2. LEHMAN REPRESENTATION AND GENERALIZED TIGHT BINDING METHOD

According to the Lehman exact spectral representation [19], the one-electron Green function with spin projection σ at $T = 0$ can be written in the form

$$G_\sigma(k, \omega) = \sum_m \left(\frac{A_{\sigma m}(k, \omega)}{\omega - \Omega_m^+} + \frac{B_{\sigma m}(k, \omega)}{\omega - \Omega_m^-} \right),$$

where the quasiparticle energy is given by

$$\Omega_m^+ = E_m(N+1) - E_0(N) - \mu,$$

$$\Omega_m^- = E_0(N) - E_m(N-1) - \mu,$$

and the spectral weights of quasiparticles are determined by the matrix elements

$$A_{\sigma m}(k, \omega) = \left| \langle 0, N | a_{k\sigma} | m, N+1 \rangle \right|^2,$$

$$B_{\sigma m}(k, \omega) = \left| \langle m, N-1 | a_{k\sigma} | 0, N \rangle \right|^2.$$

Here, $|m, N\rangle$ indicates the multielectron eigenstate of the system with N electrons and serial number m,

$$H|m, N\rangle = E_m|m, N\rangle,$$

and index m labels a quasiparticle with a spin of 1/2, charge e, energy $\Omega_m^+(\Omega_m^-)$, and spectral weight $A_{\sigma m}$ $(B_{\sigma m})$.

The Lehman representation describes an electron as a superposition of different quasiparticles for which index m is the band index of the quasiparticle.

At finite temperatures, the Lehman representation can be written, for example, for the retarded Green function (see [20, 21]) in the form

$$G_\sigma(k, \omega) = \sum_{m, n} W_n \frac{A_{\sigma, mn}(k, \omega)}{\omega - \Omega_{mn}^+} \left[1 + \exp\left(-\frac{\Omega_{mn}^+}{T} \right) \right].$$

Here,

$$\Omega_{mn}^+ = E_m(N+1) - E_n(N) - \mu$$

and the statistical weight of state $|n\rangle$ is determined by the Gibbs distribution with thermodynamic potential Ω,

$$W_n = \exp\frac{\Omega - E_n + \mu N}{T}.$$

Since not only the ground state $|0, N\rangle$, but also excited states $|n, N\rangle$ are populated at $T \neq 0$, a quasiparticle is labeled by two indices m and n and is defined as an excitation in the multielectron system associated with an addition of an electron to an N-electron system in state $|n, N\rangle$, which is accompanied by a transition to the final state $|m, N+1\rangle$.

In the Lehman representation, $|m, N\rangle$ is an unknown state of the entire crystal. In the algorithm of the GTB method, the Lehman representation is implemented in perturbation theory. Local Green's function $G^{(0)}$ has the same structure, but is determined by local multielectron terms $|m, N\rangle$. In our case, for $LaCoO_3$, the energy levels with $N = 5$, 6, and 7 corre-

sponding to configurations d^5, d^6, and d^7 of cobalt ion are significant.

We write the Hamiltonian in the generalized multiband Hubbard model in the form

$$H = H_0 + H_1, \quad H_0 = \sum_f H_c(f),$$

$$H_1 = \sum_{fg} H_{cc}(f, g),$$

where $H_c(f)$ is the intracellular part of Hamiltonian H and $H_{cc}(f, g)$ describes the jump and interaction between the fth and gth cells. We can schematically represent the GTB method as a sequence of the following three steps.

(a) Using exact diagonalization of the intracellular part $H_c(f)$ of the Hamiltonian, multielectron eigenstates $|m, N\rangle \equiv |p\rangle$ are determined for various sectors of the Hilbert space labeled by number N of electrons in a cell. A method for constructing such a set of wave eigenfunctions in the secondary quantization representation [22] taking into account electron correlations, spin−orbit interaction, and covalence was described in our previous publication.

(b) The X-operator at site f is defined as

$$X_f^{pq} = |p\rangle\langle q| = |m, N\rangle\langle m', N'|.$$

We assume that eigenstates $|p\rangle$ for neighboring cells are orthogonal. Otherwise (like for cobaltites in which two adjacent CoO_6 clusters contain a common oxygen atom), the orthogonalization procedure must be used. For $LaCoO_3$, we explicitly wrote Vanier functions instead of oxygen-group molecular orbitals classified in accordance with irreducible representations of the O_h group.

In the standard notation of X-operators, we are dealing with cumbersome and awkward notation for the initial and final states. To simplify this notation, we will employ Zaitsev's idea [23] and introduce the so-called root vector $(p, q) \longleftrightarrow \alpha(p, q) \equiv \alpha$ instead of the pair of indices (p, q). Moreover, since the set of such vectors is countable, we will label each of these vectors as $\alpha \longleftrightarrow \alpha_n$ and will henceforth indicate only the number n of the root vector:

$$X_f^{pq} \longleftrightarrow X_f^{\alpha(p, q)} \longleftrightarrow X_f^{\alpha_n} \longleftrightarrow X_f^n.$$

We define vectors α so that they correspond to electron annihilation (i.e., $N_q - N_p = +1$). Then the annihilation (production) operators for an electron in state $|f\lambda\sigma\rangle$ can be written exactly in the X-representation in the form

$$a_{f\lambda\sigma} = \sum_n \gamma_{\lambda\sigma}(n)X_f^n,$$

$$a_{f\lambda\sigma}^\dagger = \sum_n \gamma_{\lambda\sigma}^*(n)(X_f^n)^\dagger, \tag{1}$$

$$\gamma_{\lambda\sigma}(n) = \langle p|a_{f\lambda\sigma}|q\rangle.$$

Index λ runs through the entire set of the electron orbitals considered here.

(c) In the representation of X-operators, the total Hamiltonian assumes the form

$$H = \sum_{f, p} E_p X_f^{pp} + \sum_{fg} \sum_{nn'} t_{fg}^{nn'} X_f^{\dagger n} X_g^{n'}. \tag{2}$$

Since Hamiltonian H_c in the representation of Hubbard operators has a diagonal form, the local Green function can be calculated directly and is given by

$$G_{\lambda\sigma}^{(0)}(k, \omega) = \sum_n |\gamma_{\lambda\sigma}(n)|^2 \frac{F(n)}{\omega - \Omega_n}, \tag{3}$$

where $\Omega_n = E_{m'}(N + 1) - E_m(N)$ and the filling factor is $F(n) = \langle X_f^{pp} \rangle + \langle X_f^{qq} \rangle$.

Obviously, Green's function (3) implements the Lehman representation in the unit cell; however, in contrast to energies and matrix elements in the Lehman representation, which cannot be estimated, all quantities appearing in expression (3) can be calculated in terms of the local characteristics of energy levels. Here, index n denotes quasiparticles with charge e, a spin of 1/2, energy Ω_n, and spectral weight

$$A_{\lambda\sigma}(n) = |\gamma_{\lambda\sigma}(n)|^2 F(n).$$

At the same time, in view of the completeness of the basis of multielectron states $|p\rangle$, the total spectral weight is preserved in the same way as for free electrons. The obvious similarity between expression (2) and the Hamiltonian in the Hubbard model makes it possible to apply many methods in perturbation theory in parameter $t/U \ll 1$, which are familiar in the Hubbard model.

In the diagrammatic technique for X-operators [24, 25], the series in perturbation theory are constructed not for the electron Green function

$$G_{\lambda\lambda', \sigma}(k, \omega) = \langle\langle a_{k\lambda\sigma} a_{k\lambda'\sigma}^\dagger \rangle\rangle,$$

but for the matrix Green function

$$D_{nn'}(k, \omega) = \langle\langle X_k^n | (X_k^{n'})^\dagger \rangle\rangle_\omega,$$

which are connected, by virtue of relations (1), by the equality

$$G_{\lambda\lambda', \sigma}(k, \omega) = \sum_{n, n'} \gamma_{\lambda\sigma}(n)\gamma_{\lambda'\sigma}^*(n') D_{nn'}(k, \omega).$$

We can express in terms of the Fermi one-particle Green function the spectral density of one-particle excitations,

$$A_\sigma(k, \omega) = -\frac{1}{\pi} \sum_{\lambda, n, n'} \gamma_{\lambda\sigma}(n)\gamma_{\lambda\sigma}^*(n')$$

$$\times \operatorname{Im} D_{nn'}(k, \omega + i\delta) = -\frac{1}{\pi}\sum_\lambda \operatorname{Im}(G_{\lambda\lambda, \sigma}(k, \omega)),$$

and the density of one-particle states for the given spin projection

$$N_\sigma(\omega) = \frac{1}{N_k}\sum_k A_\sigma(k, \omega)$$

(N_k is the normalization factor).

For Green's function $\hat{D}$, we can write the generalized Dyson equation [24]

$$\hat{D}_\sigma(k, \omega) = \{[G_\sigma^0(k, \omega)]^{-1} + \hat{\Sigma}_\sigma(k, \omega)\}^{-1} \times \hat{P}_\sigma(k, \omega). \tag{4}$$

Here, $\hat{\Sigma}_\sigma(k, \omega)$ and $\hat{P}_\sigma(k, \omega)$ are the mass and force operators, respectively. The presence of the force operator is connected with the spectral weight redistribution and is an SEC effect. Green's function $G_\sigma^0(k, \omega)$ in Eq. (4) is defined by the relation

$$[\hat{G}_\sigma^0(k, \omega)]^{-1} = \hat{G}_0^{-1}(\omega) - \hat{P}_\sigma(k, \omega)\hat{T}_\sigma(k),$$

where $\hat{G}_0(\omega)$ is the local (intracellular) propagator and $\hat{T}_\sigma(k)$ is the matrix element of the interaction.

In the Hubbard I approximation, the structure of exact Green's function (4) is preserved, but the mass operator is set at zero, while force operator $P_\sigma^{mn}(k, \omega) \longrightarrow P_{0\sigma}^{mn} = \delta_{mn}F_\sigma^m$, where

$$F_\sigma^m \equiv F(p, q) = \langle X_f^{pp}\rangle + \langle X_f^{qq}\rangle$$

is the filling factor referred to as the end factor in the diagrammatic technique for X-operators [23]. Using the Hubbard I approximation, we obtain from Eq. (4)

$$\hat{D}_\sigma^{(0)}(k, \omega) = \{\hat{G}_0^{-1}(\omega) - \hat{P}_{0\sigma}\hat{T}_\sigma(k)\}^{-1}\hat{P}_{0\sigma}.$$

As a result, we obtain the following dispersion equation from the dispersion relation for quasiparticles:

$$\det\|\delta_{nn'}(\omega - \Omega_n)/F(n) - T_{nn'}(k)\| = 0.$$

This equation resembles in its form the dispersion equation in the tight binding method in the one-electron band theory and differs from it in the following aspects: indices m and n label one-particle excitations (quasiparticles) in a multielectron system; local energies Ω_n now contain intracellular Coulomb interactions and not one-electron energies; the band structure of quasiparticles depends on the electron concentration, temperature, and external fields via filling factors $F(n)$; and the hard band for quasiparticles cannot exist in the one-electron model.

To determine the occupation numbers and factors $F(n)$, we must solve the equation for the chemical potential, which can be written in the X-representation in the form

$$N_e = \sum_{f, m, N} N\langle X_f^{mN, mN}\rangle.$$

Here, $\langle X_f^{mN, mN}\rangle$ is the occupation number for energy level with number m of configuration d^N at site f; each term of configuration d^N makes a contribution equal to N to the number of electrons, and the sum of these contributions over all states is equal to the number of electrons N_e.

3. ONE-ELECTRON BAND STRUCTURE OF LaCoO$_3$ AND PARAMETERS OF THE MULTIBAND HAMILTONIAN

The results of calculations based on the GTB method depend quantitatively on the set of the macroscopic parameters used (such as metal–oxygen t_{pd} and oxygen—oxygen t_{pp} hopping integrals). Using the formalism of Vanier functions, we can calculate the parameters of the corresponding model on the basis of the actual crystalline structure of the systems under investigation and thus relating the model approach to characteristic features of actual chemical compounds. Figure 1 shows the results of LDA calculations of the band structure of LaCoO$_3$ in the basis of linearized muffin-tin orbitals (LMTOs) [26] using structural data [27]. The LDA bands themselves obtained without taking into account SECs beforehand describe the metal state incorrectly, which is typical of LDA calculations for all 3D oxides with SEC effects. We use LDA functions $\psi_\lambda(k)$ to calculate the Vanier functions with the help of projection technique [28] (one-electron parameters of the tight binding Hamiltonian are calculated in the basis of these functions). The band structure shown by dashed curves in Fig. 1 is also calculated using these parameters. The coincidence of the results of two different calculations indicates the reliability of the calculated hopping parameters and one-center one-electron energies. These parameters are as follows: $t_{pd}^\sigma = 1.57$ eV, $t_{pd}^\pi = 0.84$ eV, $t_{pp} = 0.3$ eV, $E_{xy, yz, xz} = 2.356$ eV, $E_{3z^2-r^2, x^2-y^2} = 1.902$ eV, $E_{px} = 3.744$ eV, $E_{py} = 3.961$ eV, and $E_{pz} = 3.792$ eV.

4. ELECTRONIC STRUCTURE OF LaCoO$_3$ AT FINITE TEMPERATURES

We consider schematically the formation of the electronic structure of LaCoO$_3$ taking SEC into account. It is well known that due to such correlations, $3d$-electrons of the transition metal ion can be treated as almost localized. Therefore, we can speak of a set of ions with the d^n electron configuration ($n = 6$ for Co^{3+}) in the crystal field. As in the Mott—Hubbard insulator, the kinetic energy of an electron is much lower than its
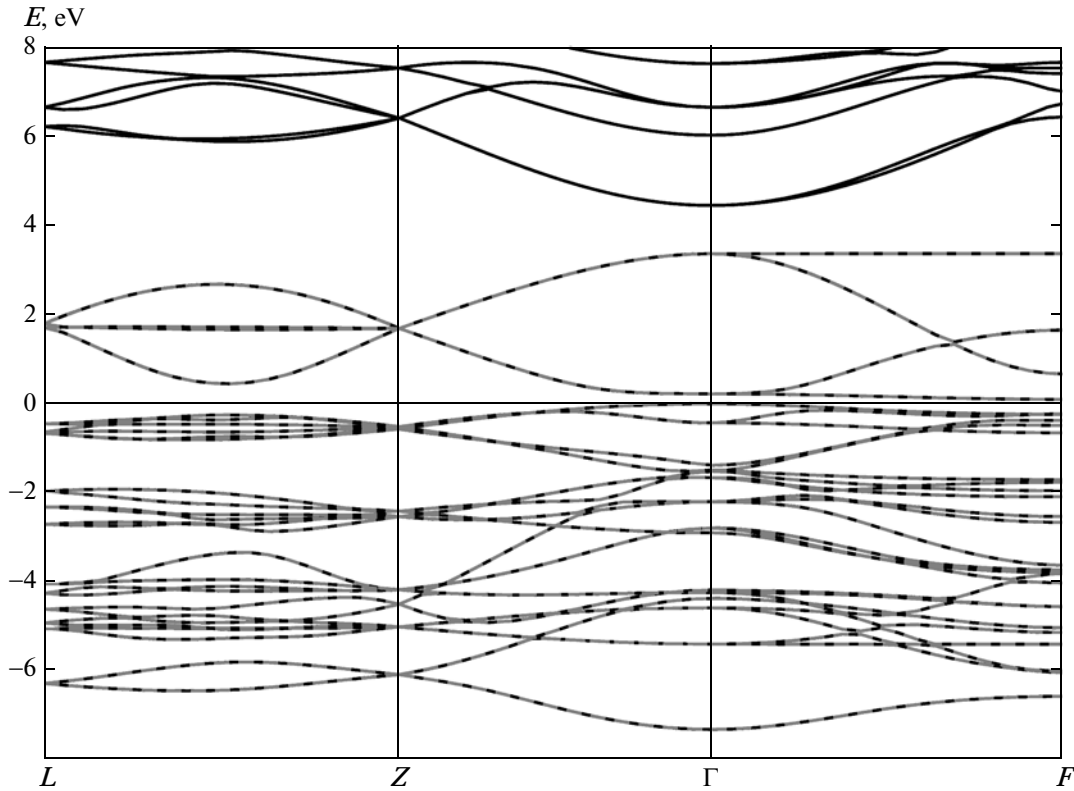
Fig. 1. Solid black and gray curves show the Band LDA structure of $LaCoO_3$. Dashed curves are bands obtained with the projection procedure for five d-orbitals of cobalt and three p-orbitals of oxygen, which completely reproduce LDA bands. The Fermi level corresponds to zero energy on the graph.

potential energy, but it still leads to charge fluctuations of the type

$$d^n + d^n \longleftrightarrow d^{n+1} + d^{n-1}. \qquad (5)$$

The existence of ligands with their electronic structure leads to the effects associated with charge transfer and fluctuations of the type

$$d^n \longleftrightarrow d^{n+1}\underline{L} \qquad (6)$$

($\underline{L}$ is the spectroscopic notation for a hole in ligands). Therefore, we must speak of the configuration of the d^n ion as a superposition of the type $d^n + d^{n+1}\underline{L}$. Such a superposition can be referred to as covalence or the covalent mixing effect. The state of an ion will henceforth be analyzed taking this superposition into account. This study is devoted to a description of propagation of perturbations (5) and (6) in $LaCoO_3$ using the Green functions and quasiparticle representations based on the GTB method. For this purpose, Fig. 2 shows the required set of low-energy terms d^n ($n = 5, 6, 7$) in the configuration of cobalt ions in an octahedral field. The well-developed mathematical apparatus of the crystal field theory makes it possible to find the position of multielectron terms of various configurations and their wavefunctions in the presence of the spin–orbit interaction and crystal field components with symmetry lower than cubic. However, the

electronic structure of ligands is disregarded in a purely ionic pattern such as crystal field theory. The above-mentioned covalent mixing was considered in [22], which is a predecessor of this work and serves as a methodological introduction. The wavefunctions of the multielectron terms in Fig. 2 were determined taking into account the orbitals of oxygen surroundings.

The position of terms in the d^6 sector ($N_e = 6$ in the figure) corresponds to that in [29]. The main term at a low temperature is the low-spin singlet $^1A_1$ separated from the triplet energy level by a gap $\Delta_{s-t} \approx 140$ K. Using this diagram, we can describe the EPR spectra for $LaCoO_3$ [30] and obtain the g-factor coinciding with the experimental value. The important general conclusion drawn in [29] is that the orbital moment in $LaCoO_3$ is "unfrozen" in contrast to that in the conventional pattern of spin magnetism in $3d$-metal oxides.

At zero temperature, only the ground term (low-spin singlet $^1A_1$) is populated; therefore, a nonzero contribution comes only from transitions (excitations) shown by solid curves in Fig. 2 (the remaining transitions are forbidden by the selection rules for spin and spin projections). Their filling factor is equal to unity. Transitions

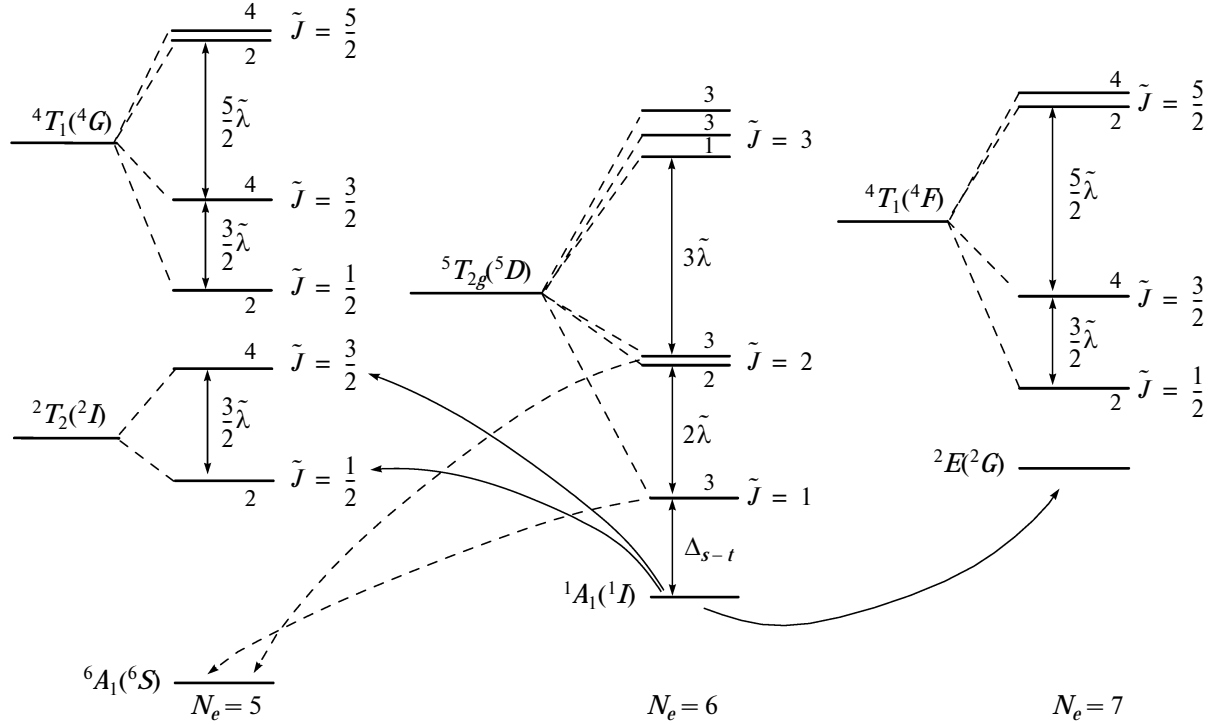$$d^6\ ^1A_1 \longrightarrow d^5\ ^2T_2\ \tilde{J} = 1/2,\ \tilde{J} = 3/2$$

Fig. 2. Set of low-energy terms for d^{N_e}, $N_e = 5, 6, 7$ electronic configurations in the crystal field. At $T = 0$, only the ground low-spin singlet $^1A_1$ ($N_e = 6$) is populated; Fermi excitations forming the bottom of the conduction bands and the top of the valence band are shown by solid lines. The dashed lines mark the transitions responsible for the formation of gap states upon an increase in temperature. Their spectral weight is determined by the population of the high-spin state of the d^6-configuration.

with energies

$$\Omega_{V1} = E(d^6, {}^1A_1) - E(d^5, {}^2T_2, \tilde{J} = 1/2),$$

$$\Omega_{V2} = E(d^6, {}^1A_1) - E(d^5, {}^2T_2, \tilde{J} = 3/2)$$

form the valence band, while transitions

$$d^6 \, {}^1A_1 \longrightarrow d^7 \, {}^2E,$$

$$\Omega_C = E(d^7, {}^2E) - E(d^6, {}^1A_1)$$

form the conduction band (Fig. 3). The transition energies determine the positions of the centers of bands. The valence band is completely filled, and the chemical potential lies in a gap of width $E_g \approx 1.5$ eV. Obviously, bands $\Omega_{V1, 2}$ and Ω_C are analogs of the lower (LHB) and upper (UHB) Hubbard subbands in the Hubbard model.

The total spectral intensity $A(k, \omega)$ can be written as the sum of the spectral intensities

$$A(k, \omega) = \sum_\lambda A_\lambda(k, \omega),$$

where index λ labels orbitals of a transition metal ion as well as group oxygen orbitals classified into the lines of irreducible representations e_g and t_{2g} of the O_h group. It can be seen that the nonzero contribution comes

from the orbitals of the e_g subsystem for the conduction band and from the orbitals of the t_{2g} subsystem for the valence band. Indeed, writing wavefunctions $|p\rangle$ of the energy levels shown in Fig. 2 in the secondary quantization representation [22] explicitly, we can calculate matrix elements $\gamma_{\lambda\sigma}(m) = \langle p|a_{\lambda\sigma}|q\rangle$ of the transition amplitude of the corresponding root vectors $\alpha_m(pq)$. The nonzero matrix elements for the transitions $d^6 \, {}^1A_1 \longrightarrow d^7 \, {}^2E$ are those for which $\lambda = x^2 - y^2$, $3z^2 - r^2$, while for the transitions $d^6 \, {}^1A_1 \longrightarrow d^5 \, {}^2T_2$, $\tilde{J} = 1/2, \tilde{J} = 3/2$, these are the matrix elements for which $\lambda = xy, yz, xz$.

Upon an increase in temperature, the quasiparticle spectrum experiences considerable modifications. The thermal population of sublevels $\tilde{J} = 1$ and $\tilde{J} = 2$ of the $^5T_2$ term increases and, as a result, contributions from various transitions which are not forbidden by the selection rule for spin and spin projections appear. The transitions

$$d^6 \, {}^5T_2 \, \tilde{J} = 1, \quad \tilde{J} = 2 \longrightarrow d^5 \, {}^6A_1$$

shown by the dashed lines in Fig. 2 with energy

$$\Omega_{V1}^* = E(d^6, {}^5T_{2g}, \tilde{J} = 1) - E(d^5, {}^6A_1),$$

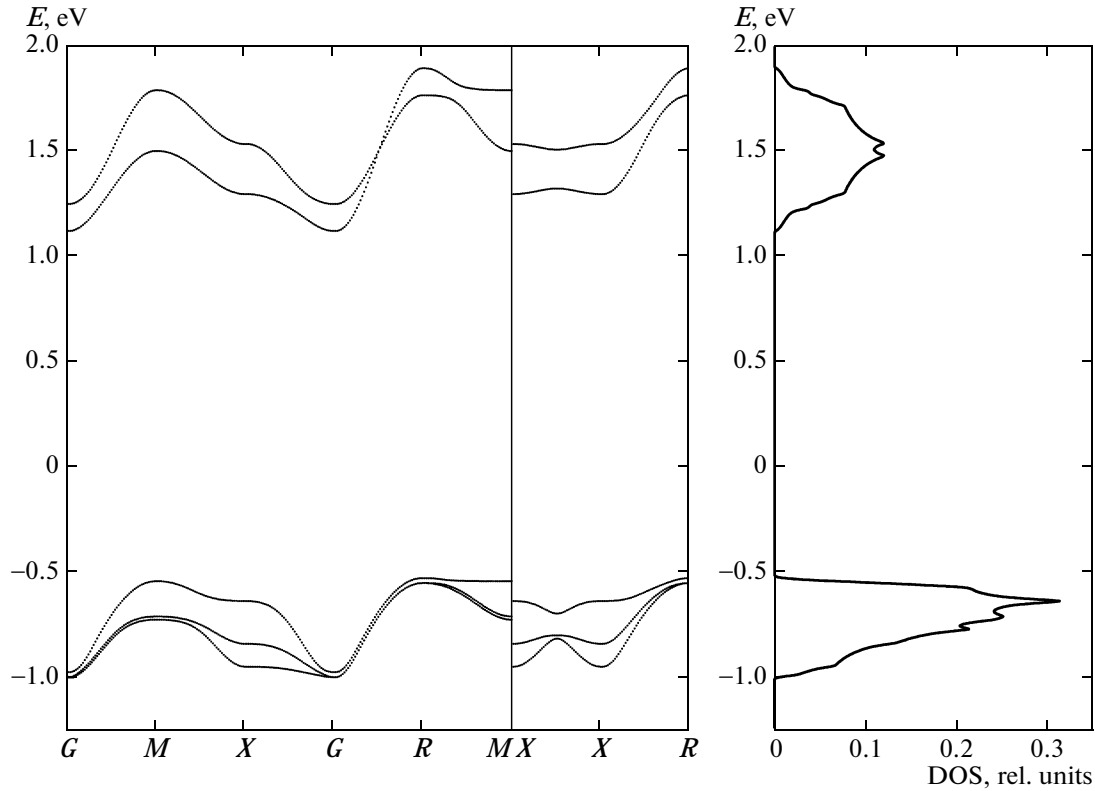$$\Omega_{V2}^* = E(d^6, {}^5T_{2g}, \tilde{J} = 2) - E(d^5, {}^6A_1)$$

Fig. 3. Quasiparticle spectrum and density of states at $T = 0$, LaCoO$_3$ is the insulator with charge transfer and gap width $E_g \approx$ 1.5 eV. $G(0, 0, 0)$, $M(\pi, \pi, 0)$, $X(\pi, 0, 0)/(0, \pi, 0)$, $R(\pi, \pi, \pi)$ are symmetric points of the Brillouin zone.

are responsible for the emergence of gap states (excitations Ω^*_{V1} and Ω^*_{V2} are larger than Ω_{V1} and Ω_{V2}, but smaller than Ω_C) and for the decrease in the dielectric gap. The results of self-consistent calculation of the band structure and the position of chemical potential μ (dashed lines) for temperatures $T = 100$ and 600 K are shown in Fig. 4. The spectral weight and the width of the band gap are proportional to the occupancies of the sublevels $\tilde{J} = 1$ and 2 of the high-spin state. At $T = 100$ K, LaCoO$_3$ preserves its dielectric properties, and the gap width is slightly larger than 0.2 eV. An increase in temperature to $T_{IMT} \approx 600$ K leads to overlapping of the bands formed by transitions $d^6\ {}^5T_2\ \tilde{J} = 1$, $\tilde{J} = 2 \longrightarrow d^5\ {}^6A_1$, $d^6\ {}^5T_2\ \tilde{J} = 1$, $\tilde{J} = 2 \longrightarrow d^7\ {}^4T_1\ \tilde{J} = 1/2$, $\tilde{J} = 3/2$, $\tilde{J} = 5/2$ and $d^6\ {}^1A_1 \longrightarrow d^7\ {}^2E$, and the dielectric gap disappears altogether (see Fig. 5) when LaCoO$_3$ acquires metallic properties.

It should be noted that the transition from the insulator to the metal (to be more precise, semimetal) state is not a phase transition in LaCoO$_3$, and the dielectric gap is not a thermodynamic order parameter.

A distinguishing feature of rare-earth cobaltites is their anomalous thermal expansion. In addition, it is well known that LaCoO$_3$ exhibits an anomalously high compressibility of length L of the Co–O bond, $\beta_L =$

$-L^{-1}(\partial L/\partial P)_T = 4.8 \times 10^{-3}$ GPa^{-1} [31]. This is a record-high value for the compressibility of the B–O bond in all ABO$_3$ perovskites. Such a high compressibility apparently leads to a strong temperature dependence of the bond lengths. For example, $L = 1.9254$ Å at $T = 5$ K and $L = 1.9446$ Å at $T = 550$ K [27]. It follows hence that the crystal field Dq must noticeably decrease upon heating. In the conventional crystal field theory, splitting $\Delta = 10$ Dq is defined as

$$\Delta = \varepsilon(E_g) - \varepsilon(T_{2g}) = \frac{5}{3}eqF_4(R),$$

where R is the distance between six negative charges q and the central atom. The authors of [32] believe that such a suppression of the crystal field leads to a decrease in Δ_{s-t} to zero at $T = 500–600$ K. In other words, a crossover takes place between the low-spin singlet ${}^1A_1$ and triplet $\tilde{J} = 1$. Such features of the behavior can be taken into account in calculating the electronic structure of LaCoO$_3$ with the help of a simple linear temperature dependence of the crystal field. Indeed, the characteristic size in atomic physics is the first Bohr radius $a_0 \approx 0.53$ Å, and the change in the length of the Co–O bond is approximately 0.02 Å.
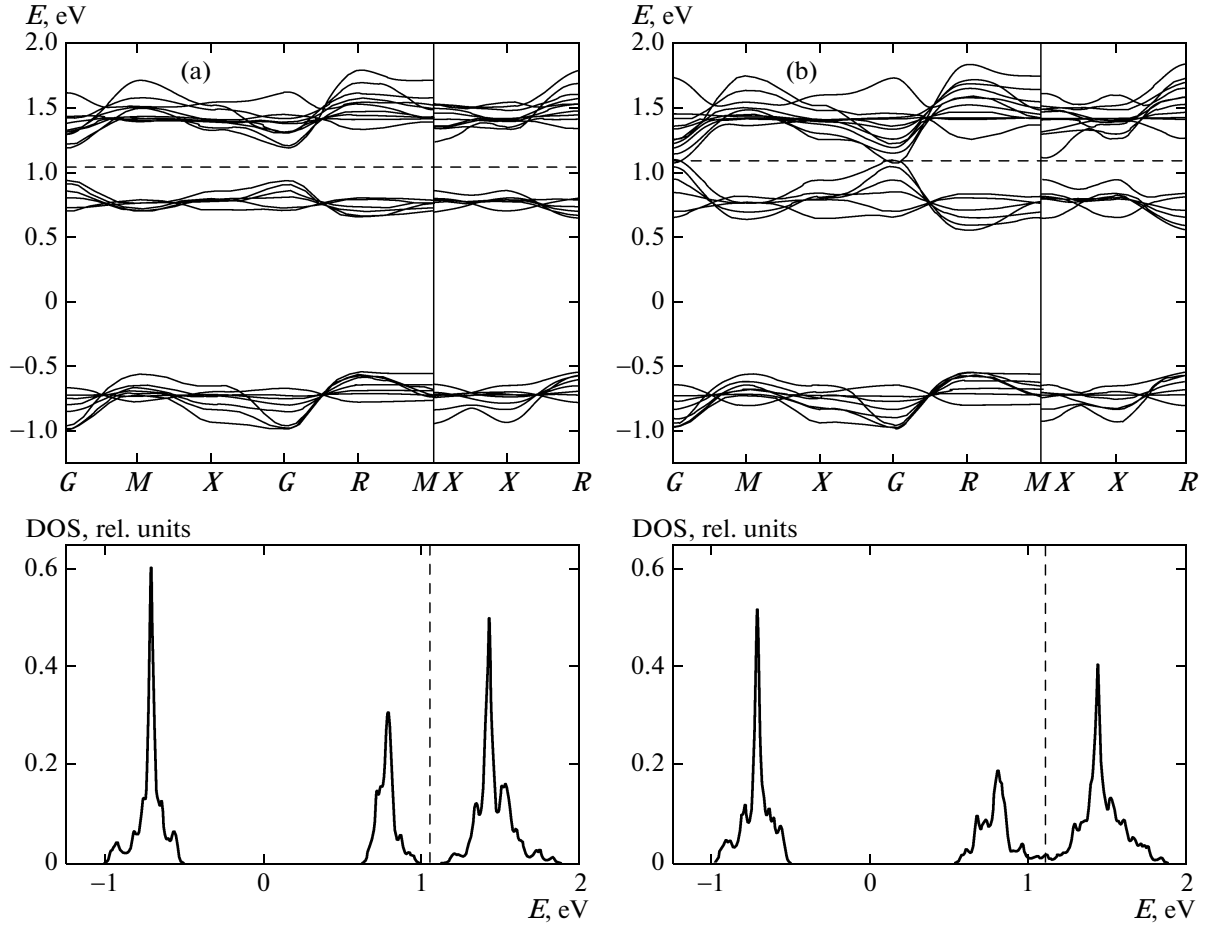
Fig. 4. Quasiparticle spectrum and density of states for two characteristic values of temperature. (a) At $T = 100$ K, the increase in the gap states is observed, while (b) at $T = 600$ K, the band structure is of the metal type.

5. ELECTRONIC PROPERTIES

5.1. Temperature Dependence of Conductivity

Assuming that the mobility of charge carriers depends on temperature, while the concentration at $T < T_{IMT}$ is determined by the activation excitation through gap E_g, we define the conductivity σ using the classical formula

$$\sigma = \sigma_0 \exp\left(-\frac{E_a}{kT}\right).$$

Here, k is the Boltzmann constant and E_a is the conduction activation energy. We try to describe the experimentally observed behavior of resistivity of LaCoO$_3$ using this formula.

The resistivity is defined as

$$\rho = \frac{1}{\sigma} = \rho_0 \exp\frac{E_g}{2kT}.$$

It is important to note that the gap width in our case is a function of temperature (see Fig. 5). The value of ρ_0 is taken from experiment at $T = 800$ K.

The results of calculations and experimental data [11] are compared in Fig. 6. It can be seen that the theoretical curve describes the general regularity excluding the singularity at $T \approx 300$ K. This discrepancy can be due to additional interactions disregarded by us. For example, the thermal expansion coefficient has a similar singularity in the same temperature range [33]; consequently, the spin–phonon and the electron–phonon interactions are probably responsible for the observed discrepancy.

5.2. Temperature Dependence of the Average Magnetic Moment

Let $\hat{Q}$ be an arbitrary operator. The representation of the one-site operators in terms of the Hubbard operators can be written in the simplest form using the Dirac notation. This gives

$$\hat{Q} = \hat{1} \cdot \hat{Q} \cdot \hat{1} = \sum_{pq} |p\rangle\langle p|\hat{Q}|q\rangle\langle q| = \sum_{pq} \langle p|\hat{Q}|q\rangle X^{pq},$$
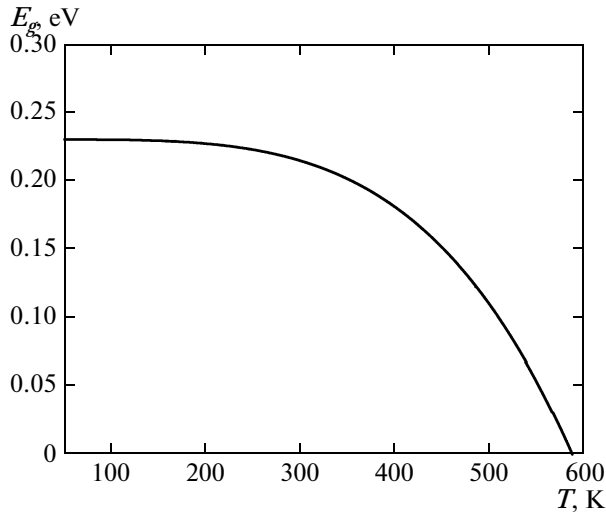
Fig. 5. Temperature dependence of dielectric gap width E_g; $E_g = 0$ at $T = T_{IMT} \approx 587$ K.

where matrix element $\langle p|\hat{Q}|q\rangle$ can be treated as the classical quantitative measure determining the intensity of the transition from state $|q\rangle$ to state $|p\rangle$ under the physical action described by operator $\hat{Q}$. Ket vectors $|p\rangle$ and $|q\rangle$ define, as before, the complete set of orthonormal or one-cell eigenstates.

For operator $\hat{Q}$, we take the square of the operator of the total angular momentum. Then we obtain the following expression for the mean square of the angular momentum:

$$\langle\hat{J^2}\rangle = \sum_{pq}\langle p|\tilde{J^2}|q\rangle\langle X^{pq}\rangle.$$

In our case, states $|p\rangle$ and $|q\rangle$ are the eigenstates of operator $\hat{J^2}$ (see Fig. 2); therefore, we can write

$$\langle\hat{J^2}\rangle = \sum_{N}\sum_{p(N)}\langle p(N)|\hat{J^2}|p(N)\rangle\langle X^{p(N)p(N)}\rangle,$$

where the sum over N is the sum over the vectors of the Hilbert space ($N = 5, 6, 7$).

As the measure of the mean value of the angular momentum operator, we take the square root of the average value of the squared angular momentum:

$$J_{av} = \sqrt{\langle\hat{J^2}\rangle};$$

since mean values $\langle X^{pp}\rangle$ are functions of temperature, J_{av} is also a function of temperature (see Fig. 7).

At low temperatures, the average value of the angular momentum is close to zero, which corresponds to the nonmagnetic state of $LaCoO_3$. The value of $J_{av} \approx 2$ expected for the high-spin state is attained only at $T \approx 1000$ K. At a temperature of 100 K, the average value of the angular momentum is close to unity. We believe
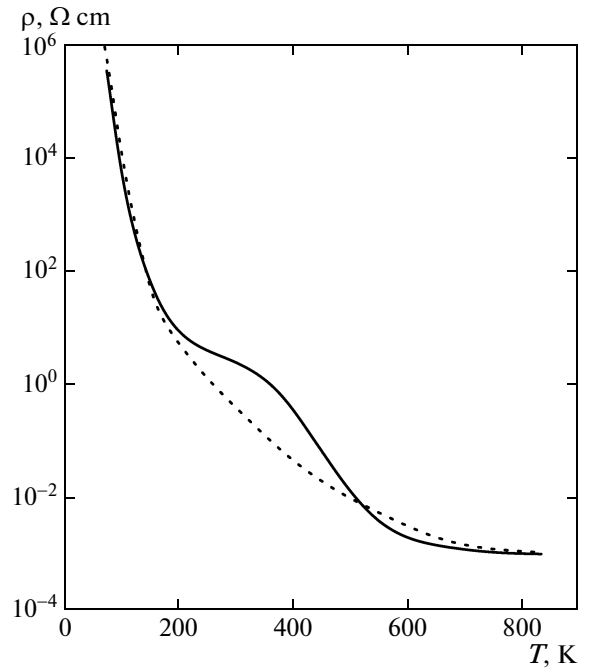

Fig. 6. Temperature dependence of resistivity. The solid curve represents experimental data [11], and the dotted curve reflects theoretical results.

that this can be the reason for the popular opinion that the intermediate state makes a decisive contribution to the spin transition in $LaCoO_3$ at 100 K.

6. MAGNETIC SUSCEPTIBILITY

In recent years, $LaCoO_3$ has attracted considerable attention because it experiences two broad magneto-electron transitions upon an increase in temperature, which are often referred to as crossovers. The first crossover, which is clearly manifested in the behavior of magnetic susceptibility χ, is considered as a spin transition. At low temperatures ($T < 30$ K), cobalt ions in $LaCoO_3$ exist in the nonmagnetic low-spin state $^1A_1$, $\chi \approx 0$. A sharp increase in the magnetic susceptibility to the maximal value near $T = 100$ K indicates thermal excitation of a state with a higher spin and with a nonzero magnetic moment. When the temperature increases above 100 K, the magnetic susceptibility decreases again. The second high-temperature crossover ($T \approx 600$ K) is observed during the insulator–metal transition.

Solving the self-consistent equation for the mean value of magnetic moment $\langle\mu\rangle$ per site in the mean field theory, the authors of [34] succeeded in describing the experimental behavior of magnetic susceptibility at $T = 200$ K taking into account short-range antiferromagnetic correlations. Only the ground nonmagnetic singlet $^1A_1$ and triplet $\tilde{J} = 1$ were taken into account, which, in the opinion of the authors of [34],
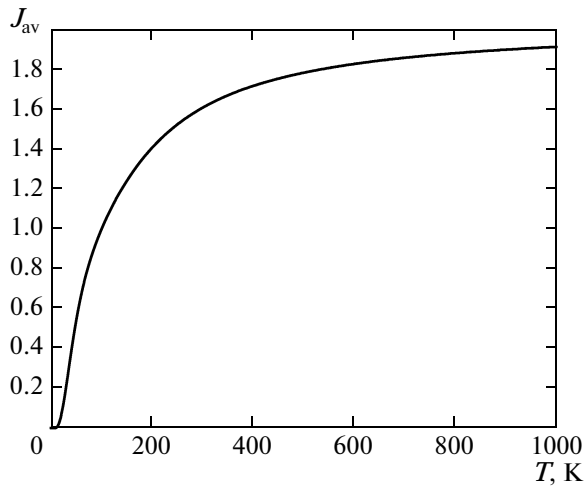
Fig. 7. Temperature dependence of average angular momentum. Transition from low-spin state at $T \approx 0$ to paramagnetic state upon heating. At spin transition temperature $T \sim 100$ K, $J_{av} \approx 1$.

limited their analysis of the temperature behavior of the material. However, in the proposed approach, the upper-lying quintet level $\tilde{J} = 2$ can also be considered easily. Following [34], we show by the solid curve in Fig. 8a the result of calculation of $\langle \mu \rangle / g\mu_B$ in a magnetic field of 10 T. The quantities used in calculations were as follows: $\Delta_{s-t} = 145$ K, uniaxial trigonal distortion (splitting in zero crystal field) $D = 7$ K, Lande factors $g = 3.4$ for triplet $\tilde{J} = 1$ and $g' = 3.1$ and $g'' = 1.8$ for quintet $\tilde{J} = 2$, and the antiferromagnetic interaction constant is $J = -28$ K. The type of the interaction between the cobalt ions in $LaCoO_3$ is not completely

clear; however, the Curie–Weiss behavior of the magnetic susceptibility typical at $T > 130$ K suggests that

the antiferromagnetic correlations considered and noted initially in [5, 11, 35] take place.

The total magnetization of $LaCoO_3$ can be written as the sum

$$M_{tot} = M_{lot} + M_{band}.$$

The first term $M_{loc} = N_A \langle \mu \rangle$ describes the contribution of localized magnetic moments of Co^{3+} ions; the second term is the band contribution of collectivized electrons observed in the vicinity of and above the transition to the metal state. To estimate this contribution, the behavior of the valance and conduction bands in the vicinity of the points of their intersection (see Fig. 4) in the temperature range near T_{IMT} is considered using the effective two-band model shown schematically in Fig. 9 with a quadratic dispersion relation $E_k = \hbar^2 k^2 / 2m^*$ and effective mass $m^* \approx 4.5 m_e$.

In a magnetic field H, bands 1 and 2 split into two subbands with opposite spin projections. The low-lying (low-energy) subband in which the spin moment of electrons is directed along the field is populated more strongly, which leads to the formation of magnetic moment $M_{band} = \chi_{Pauli} H$. Pauli susceptibility χ_{Pauli} is determined in the standard manner [36]. The dashed curve in Fig. 8a shows the Pauli contribution of band electrons to the average value of the magnetic moment per structural unit of the substance. The resultant (overall) behavior of the magnetic susceptibility (solid curve) against the background of experimental dependence [37] (dots) is show in Fig. 8b. It can be seen that both curves have similar singularities. Remarkably, the temperature plateau is associated with a smooth insulator–metal transition and is prob-
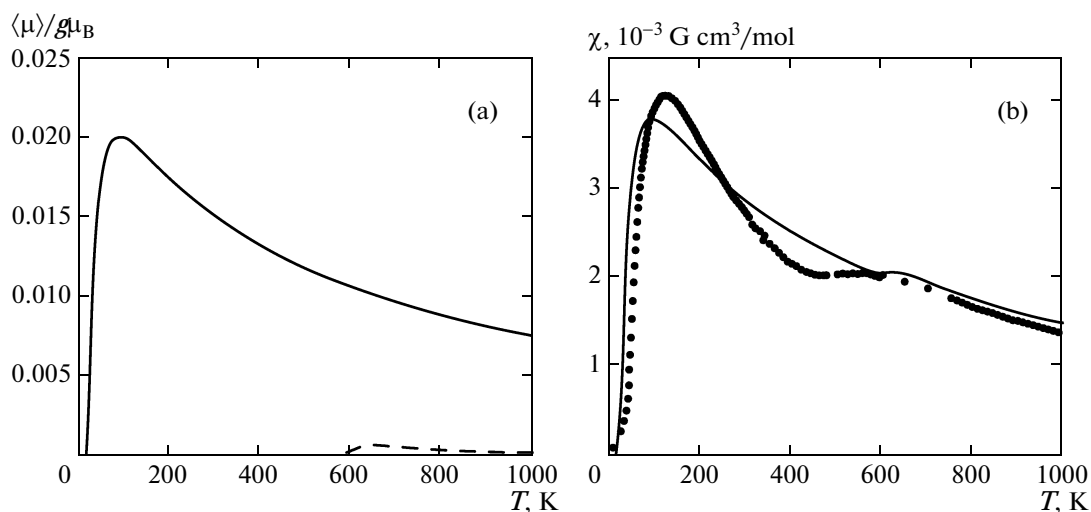

Fig. 8. (a) Average magnetic moment per site (cell) in units of Bohr magneton μ_B for localized (solid curve) and collectivized (dashed curve) electron states. (b) Curie susceptibility of Co^{3+} ions. Dots correspond to experimental dependence [37]; solid curve is the result of model calculations.
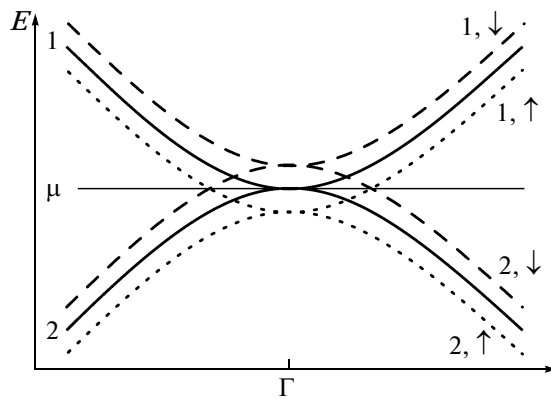
Fig. 9. Effective two-band model for analyzing the Pauli magnetization. In the magnetic field, bands 1 and 2 (solid curves) split into two subbands (dotted and dashed curves) with opposite spin projections; μ is the position of the chemical potential.

ably due to the emergence of additional magnetization from conduction electrons.

7. CONCLUSIONS

The Hubbard model describes transition metals in which atomic magnetic moments of $3d$-shells are partly collectivized in the crystal so that the same d-electrons are responsible for conduction (together with s-electrons of the outer atomic shell) and for local magnetic moments. This model simplified so that fine details are disregarded makes it possible to describe the most general effects in substances with SECs. If a more detailed description of a narrow group of substances is required, the model can be extended by adding multiorbital schemes and specific interactions (e.g., magnetic anisotropy, spin−orbit interaction, and crystal field). Various types of interaction and covalence effects were taken into account in analyzing the properties and electronic structure of $LaCoO_3$. The correct description of an electron in a strongly correlated system in the form of a linear combination of quasiparticle excitations between various multielectron states makes it possible to calculate and analyze the behavior of the band structure. The mathematical language that makes such an approach possible is the representation of Hubbard X-operators. The spectral weight of quasiparticle excitations is determined by the population of local multielectron states. For example, in the case of $LaCoO_3$, gap states associated with transitions from the high-spin state of the d^6-configuration to the high-spin state of the d^5 configuration are of special interest. With increasing temperature, the contribution from such states becomes decisive, which leads to a decrease in the dielectric gap width and ultimately to the insulator−metal transition. Thus, in spite of the temperature difference between the spin transition ($T = 80-120$ K) and the metal−insulator transition ($T = 500-600$ K), the basic mechanism of

these effects remains unchanged and is determined by the thermal population of the $^5T_{2g}$ high-spin state.

REFERENCES

1. N. B. Ivanova, S. G. Ovchinnikov, M. M. Korshunov, I. M. Eremin, and N. V. Kazak, Usp. Fiz. Nauk **179** (8), 837 (2009) [Phys.—Usp. **52** (8), 789 (2009)].

2. A. A. Taskin, A. N. Lavrov, and Y. Ando, Phys. Rev. Lett. **90**, 227201 (2003).

3. W. Kobayashi, S. Ishiwata, I. Terasaki, M. Takano, I. Grigoraviciute, H. Yamauchi, and M. Karppinen, Phys. Rev. B: Condens. Matter **72**, 104408 (2005).

4. Y. Moritomo, M. Takeo, X. J. Liu, T. Akimoto, and A. Nakamura, Phys. Rev. B: Condens. Matter **58**, R13334 (1998).

5. D. Phelan, Despina Louca, S. Rosenkranz, S.-H. Lee, Y. Qiu, P. J. Chupas, R. Osborn, H. Zheng, J. F. Mitchell, J. R. D. Copley, J. L. Sarrao, and Y. Moritomo, Phys. Rev. Lett. **96**, 027201 (2006).

6. J. Baier, S. Jodlauk, M. Kriener, A. Reichl, C. Zobel, H. Kierspel, A. Freimuth, and T. Lorenz, Phys. Rev. B: Condens. Matter **71**, 014443 (2005).

7. V. P. S. Awana, J. Nakamura, M. Karppinen, H. Yamauchi, and S. K. Malik, J. Magn. Magn. Mater. **250**, 6 (2002).

8. N. B. Ivanova, N. V. Kazak, C. R. Michel, A. D. Balaev, S. G. Ovchinnikov, A. D. Vasil'ev, N. V. Bulina, and E. B. Panchenko, Fiz. Tverd. Tela (St. Petersburg) **49** (8), 1427 (2007) [Phys. Solid State **49** (8), 1498 (2007)].

9. A. Podlesnyak, M. Russina, A. Furrer, A. Alfonsov, E. Vavilova, V. Kataev, B. Büchner, Th. Strässle, E. Pomjakushina, K. Conder, and D. I. Khomskii, Phys. Rev. Lett. **101**, 247603 (2008).

10. V. G. Bhide, D. S. Rajoria, G. Rama Rao, and C. N. R. Rao, Phys. Rev. B: Solid State **6**, 1021 (1972).

11. S. Yamaguchi, Y. Okimoto, H. Taniguchi, and Y. Tokura, Phys. Rev. B: Condens. Matter **53**, R2926 (1996).

12. M. Abbate, J. C. Fuggle, A. Fujimori, L. H. Tjeng, C. T. Chen, R. Potze, G. A. Sawatzky, H. Eisaki, and S. Uchida, Phys. Rev. B: Condens. Matter **47**, 16124 (1993).

13. K. Asai, P. Gehring, H. Chou, and G. Shirane, Phys. Rev. B: Condens. Matter **40**, 10982 (1989).

14. S. Yamaguchi, Y. Okimoto, and Y. Tokura, Phys. Rev. B: Condens. Matter **54**, R11 022 (1996).

15. M. W. Haverkort, arXiv:cond-mat/0505214v1.

16. S. G. Ovchinnikov, Zh. Eksp. Teor. Fiz. **134** (1), 172 (2008) [JETP **107** (1), 140 (2008)].

17. S. G. Ovchinnikov and I. S. Sandalov, Physica C (Amsterdam) **161**, 607 (1989).

18. M. M. Korshunov, V. A. Gavrichkov, S. G. Ovchinnikov, I. A. Nekrasov, Z. V. Pchelkina, and V. I. Anisimov, Phys. Rev. B: Condens. Matter **72**, 165 104 (2005).

19. H. Lehman, Nuovo Cimento **11**, 342 (1954).

20. A. A. Abrikosov, L. P. Gor'kov, and I. E. Dzyaloshinskii, *Quantum Field Theoretical Methods in Statistical Physics* (Fizmatgiz, Moscow, 1962; Pergamon, Oxford, 1965).

21. D. N. Zubarev, Usp. Fiz. Nauk **71**, 71 (1960) [Sov. Phys.—Usp. **3**, 320 (1960)].

22. Yu. S. Orlov and S. G. Ovchinnikov, Zh. Eksp. Teor. Fiz. **136** (2), 377 (2009) [JETP **109** (2), 322 (2009)].

23. R. O. Zaitsev, Zh. Eksp. Teor. Fiz. **70** (4), 1100 (1976) [Sov. Phys. JETP **43** (4), 574 (1976)].

24. V. V. Val'kov and S. G. Ovchinnikov, *Quasiparticles in Strongly Correlated Systems* (Siberian Branch of the Russian Academy of Sciences, Novosibirsk, 2001) [in Russian].

25. Yu. A. Izyumov, M. I. Katsnel'son, and Yu. N. Skryabin, *Magnetism of Itinerant Electrons* (Fizmatgiz, Moscow, 1994) [in Russian].

26. O. K. Andersen and O. Jepsen, Phys. Rev. Lett. **53**, 2571 (1984).

27. P. G. Radaelly and S. W. Cheong, Phys. Rev. B: Condens. Matter **66**, 094 408 (2002).

28. V. I. Anisimov, D. E. Kondakov, A. V. Kozhevnikov, I. A. Nekrasov, Z. V. Pchelkina, J. W. Allen, S.-K. Mo, H.-D. Kim, P. Metcalf, S. Suga, A. Sekiyama, G. Keller, I. Leonov, X. Ren, and D. Vollhardt, Phys. Rev. B: Condens. Matter **71**, 125119 (2005).

29. Z. Ropka and R. J. Radwanski, Phys. Rev. B: Condens. Matter **67**, 172401 (2003).

30. S. Noguchi, S. Kawamata, and K. Okuda, Phys. Rev. B: Condens. Matter **66**, 094404 (2002).

31. T. Vogt, J. A. Hriljac, N. C. Hyatt, and P. Woodward, Phys. Rev. B: Condens. Matter **67**, 140 401 (2003).

32. R. J. Radwanski and Z. Ropka, arXiv:cond-mat//0404713v1.

33. K. Asai, O. Yokokura, and N. Nishimori, Phys. Rev. B: Condens. Matter **50**, 3025 (1994).

34. M. J. R. Hoch, S. Nellutla, J. van Tol, Eun Sang Choi, Jun Lu, H. Zheng, and J. F. Mitchell, Phys. Rev. B: Condens. Matter **79**, 214421 (2009).

35. M. A. Senaris-Rodriguez and J. B. Goodenough, J. Solid State Chem. **116**, 224 (1995).

36. N. Ashcroft and N. Mermin, *Solid State Physics* (Holt, Rinehart and Winston, New York, 1976; Mir, Moscow, 1979), Vol. 2.

37. J. Baier, S. Jodlauk, M. Kriener, A. Reichl, C. Zobel, H. Kierspel, A. Freimuth, and T. Lorenz, Phys. Rev. B: Condens. Matter **71**, 014443 (2005).

Translated by N. Wadhwa